





Article

Svetlanaite, SnSe, a new mineral from the Ozernovskoe deposit, Kamchatka peninsula, Russia

Victor M. Okrugin¹, Anna Vymazalová^{2*} , Vladimir V. Kozlov³ , František Laufek², Chris J. Stanley⁴
and Ilya A. Shkilev⁵

¹Institute of Volcanology and Seismology, Russian Academy of Science, Petropavlovsk-Kamchatsky, 683006, Russia; ²Czech Geological Survey, Geologická 6, 152 00 Prague, Czech Republic; ³Oxford Instruments (Moscow Office), 26, Denisovskii Pereulok, Moscow, 105005, Russia; ⁴Department of Earth Sciences, Natural History Museum, London SW7 5BD, UK; and ⁵JSC “Siberian Mining and Metallurgical Alliance”, Mishennaya 106, Petropavlovsk-Kamchatsky, Kamchatka Territory, 683016, Russia

Abstract

Svetlanaite, SnSe is a new mineral discovered from the high-sulfidation epithermal Au-deposit Ozernovskoe, Kamchatka peninsula, Russia. It forms tiny euhedral spindles (0.5–2 μm × 10–15 μm) in quartz, in close association with cassiterite, rutile, mawsonite, kiddcreekite, hemusite, tellurium, kostovite and Se-bearing ‘fahlores’ (Se-goldfieldite–Se(Bi)-tetrahedrite–Se-tennantite). In plane-polarised light, svetlanaite is light-grey, pleochroic from white to cream and strongly anisotropic in shades of light blue, dark blue, khaki and orange-brown; it exhibits no internal reflections. Reflectance values of synthetic analogue of svetlanaite in air (R_1 , R_2 in %) are: 50.9, 56.5 at 470 nm, 50.2, 56.7 at 546 nm, 49.5, 55.3 at 589 nm and 48.7, 53.4 at 650 nm. Twelve electron-microprobe analyses of svetlanaite give an average composition: Sn 61.30, Se 37.22 and S 1.25 total 99.79 wt.%, corresponding to the empirical formula $\text{Sn}_{1.01}(\text{Se}_{0.92}\text{S}_{0.07})_{\Sigma 0.99}$ based on 2 atoms; the average of seven analyses on its synthetic analogue is: Sn 59.98 and Se 39.71, total 99.59 wt.%, corresponding to $\text{Sn}_{1.00}\text{Se}_{1.00}$. The density, calculated on the basis of the empirical formula, is 6.08 g/cm³. The mineral is orthorhombic, space group *Prima*, with $a = 11.500(2)$, $b = 4.154(2)$, $c = 4.445(2)$ Å, $V = 212.34(14)$ Å³ and $Z = 4$. The crystal structure was solved and refined from the powder X-ray-diffraction data of synthetic SnSe. It crystallises in the GeS-structure type. It is isostructural with the mineral herzenbergite (SnS). The mineral name is in honour of Svetlana K. Smirnova, a Russian mineralogist, for her contributions to geology in the epithermal Au–Ag deposits of the Tien–Shan region.

Keywords: svetlanaite, SnSe, electron-microprobe data, reflectance data, X-ray-diffraction data, crystal structure, Ozernovskoe deposit, Kamchatka, Russia

(Received 4 August 2021; accepted 25 October 2021; Accepted Manuscript published online: 17 February 2022; Associate Editor: Elena Zhitova)

Introduction

Svetlanaite, SnSe, is a new mineral discovered in quartz veins the Au–Te–Se volcanic-hosted high-sulfidation epithermal Au deposit, Ozernovskoe, Kamchatka peninsula, Russia (57°35′36″N, 160°50′60″E), Fig. 1. It occurs in bonanza Au–Te ores in a complex multistage mineral assemblage with quartz, cassiterite, rutile, Sn-, W- and Mo-bearing sulfides and sulfoselenides (Se-herzenbergite, Se-mohite, Se-mawsonite, Se-stannite and kiddcreekite) later followed by ore minerals chalcopyrite, ‘fahlores’ (tennantite–tetrahedrite solid-solution series minerals), Bi and Bi–Pb selenotellurides, Au, Ag and Cu tellurides and tellurium. The paragenetic sequence possibly reflects a fluid boiling process: a rapid temperature drop from 300–350°C to 150–180°C and pH

increase due to loss of H₂S and other volatiles to the gas phase. It leads to the formation of extremely rich and complex bonanza ores with banded and breccia textures.

Both mineral and name (symbol Svl) were approved by the Commission on New Minerals, Nomenclature and Classification of the International Mineralogical Association (IMA2020-013, Okrugin *et al.*, 2020). The mineral name honours Dr Svetlana Konstantinovna Smirnova (Светлана Константиновна Смирнова) (1935–2011), a Russian mineralogist, from the Institute of Geology and Geophysics, Academy of Sciences of Uzbekistan (IGG ASUz). Dr Smirnova was a specialist in the mineralogy and geology of gold deposits, in particular she worked on the epithermal Au–Ag deposits of the Tien–Shan region.

The holotype material (polished section), along with its synthetic analogue (Exp Sn1), is deposited at the Department of Earth Sciences of the Natural History Museum, London, UK, catalogue number BM 2020, 2.

According to the chemical composition, the mineral belongs to the 2.CD.10 (Metal Sulfides, M:S = 1:1) category of the Nickel and Strunz classification (Strunz and Nickel, 2001).

*Author for correspondence: Anna Vymazalová, Email: anna.vymazalova@geology.cz
Cite this article: Okrugin V.M., Vymazalová A., Kozlov V.V., Laufek F., Stanley C.J. and Shkilev I.A. (2022) Svetlanaite, SnSe, a new mineral from the Ozernovskoe deposit, Kamchatka peninsula, Russia. *Mineralogical Magazine* 86, 234–242. <https://doi.org/10.1180/mgm.2021.80>



Fig. 1. Ozernovskoe Au–Ag deposit location in the Kamchatka region, Far East of Russia.

Geological setting, occurrence and associated minerals

The Ozernovskoye deposit is located within the North Kamchatka ore region of the Central Kamchatka volcanic belt, 140 km north of the village of Klyuchi and 80 km west of the Bering Sea coast (Fig. 1).

This Au–Te–Se deposit of epithermal high sulfidation type is localised within a Miocene basaltic palaeovolcano, composed of sills and dykes of andesite–basalts, intruded by volcanic domes of andesites, andesite–dacites, dacites, magmatic breccias and tuffites (Spiridonov *et al.*, 1990; Petrenko, 1999; Litvinov *et al.*, 1999; Kovalenker and Plotinskaya, 2005; Demin, 2015).

Four prospects have been identified at the field – BAM, Intermediate, Khomut and Prometey (Fig. 2). Mineralisation is localised in steeply dipping zones of hydrothermal alteration (quartz, quartz–alunite, quartz–kaolinite–dickite metasomatites and argillites (Naumova, 1995) from 1 to 120 m thick and up to 100–1040 m long. It is associated with stockworks of quartz veinlets and hydrothermal breccias containing disseminated ore minerals (pyrite, chalcopyrite, fahlores and various tellurides and selenides of gold, silver and bismuth, etc., together with native gold). Most of the known ore bodies occur in the BAM zone, where 16 ore bodies have been identified with up to 200 ppm Au, 188 ppm Ag, 450 ppm Bi, 1143 ppm Te and 1280 ppm Se (Litvinov *et al.*, 1999). The vertical range of mineralisation is estimated at 250–300 m. The distribution of gold in ores is extremely uneven and most of it is localised in small bonanzas (Vakin and Naumova, 1994; Naumova, 1995), where it can reach 1859 ppm (Litvinov *et al.*, 1999).

Currently, three main prospects of the deposit (BAM, Khomut and Intermediate), where commercial gold ores have been

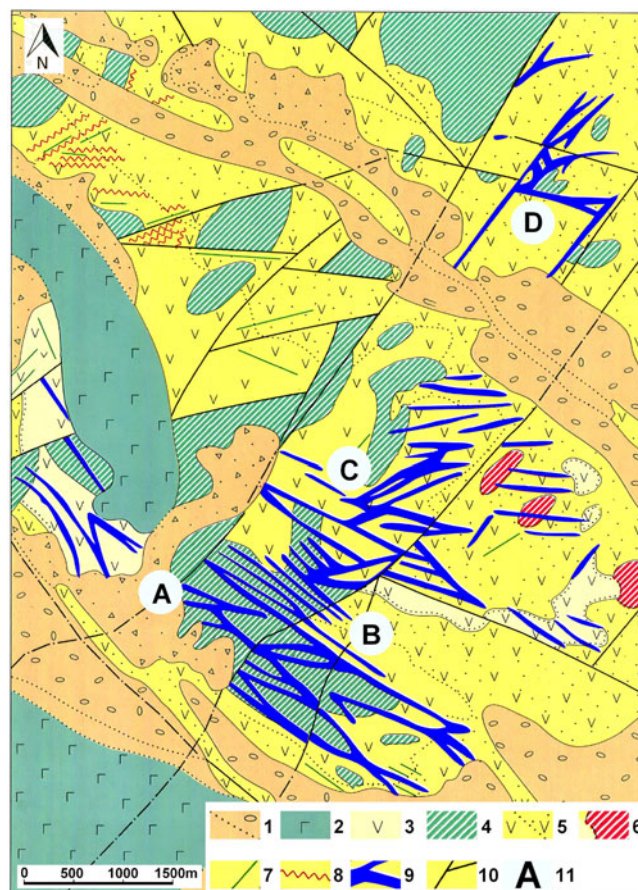


Fig. 2. Geological sketch map of the Ozernovskoe Au–Ag deposit (after Litvinov *et al.*, 1999). Legend: [1] Quaternary loose alluvial deposits; [2] Quaternary basaltic lava flows; [3] andesite lavas (N_2 – Pliocene); [4] subvolcanic bodies of andesite–basalts (N_1 – Miocene); [5] lavas and tuffs of andesites and andesite–dacites (N_1 – Miocene); [6] subvolcanic bodies of andesite–dacites (N_1 – Miocene); [7] andesite dykes, (N_1 – Miocene); [8] quartz veins; [9] ore-bearing zones of argillic and secondary dickite quartzites with quartz veins; [10] post-ore faults; and [11] designation of ore-bearing prospects: A – BAM zone; B – ‘Intermediate’; C – ‘Khomut’; D – ‘Prometheus’.

identified, are in the exploration stage by the SiGMA mining company (Demin, 2015).

Several samples from bonanzas of the BAM zone have been studied in detail by us. Ore deposition here is related to multiple repeated cycles of extensive boiling and related hydrothermal brecciation (Fig. 3). Colloform textures with bands of quartz and precious metals are the result of boiling and supersaturation (Fig. 4). From one to five stages of ore minerals deposition can be recognised on every deposition cycle (Fig. 5). Most sulfide minerals of all stages contain a varying amount of selenium replacing sulfur. Pyrite crystals often contain zones enriched in Se (up to 12 wt.%).

The above deposition sequence reflects dramatic changes of the ore-bearing fluid chemistry and temperature: from an early low-pH high-temperature (>300°C) fluid with relatively high sulfur activity (in both, H_2S and SO_2 forms) to the lower temperature (250–150°C) fluids with increased Se and then Te activity (Kovalenker and Plotinskaya, 2005) and increased pH (up to the dolomite stability field). We propose that the unusually high Se and Te activity of the later stages of the cycle could be explained partly by kinetic factors and related to the difference

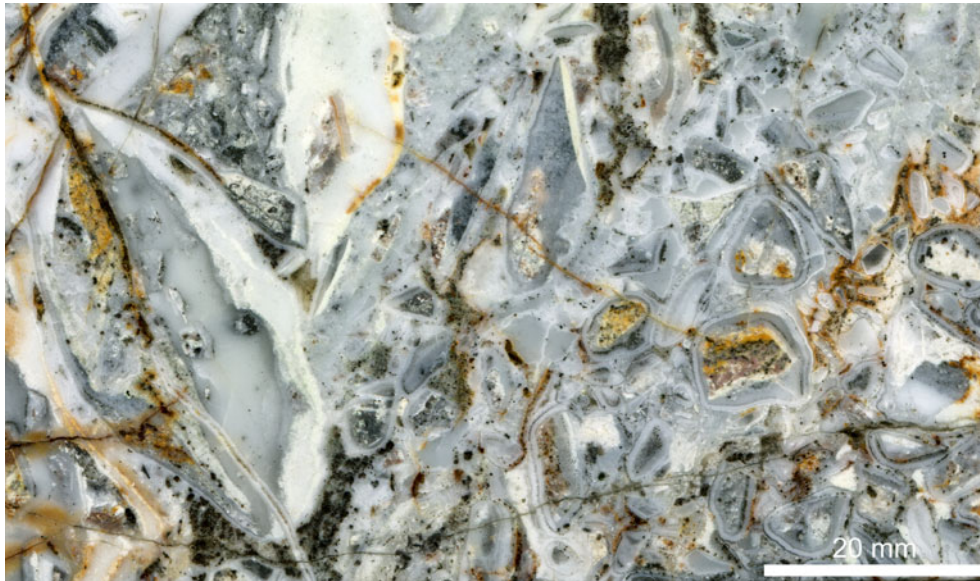


Fig. 3. Hydrothermal breccia. Clasts of altered rocks and earlier-stage banded ore-minerals bearing quartz are cemented by a matrix of quartz with disseminated pyrite. Some clasts are also breccias cementing earlier-stage clasts. BAM zone, borehole core section 14, 144 m.

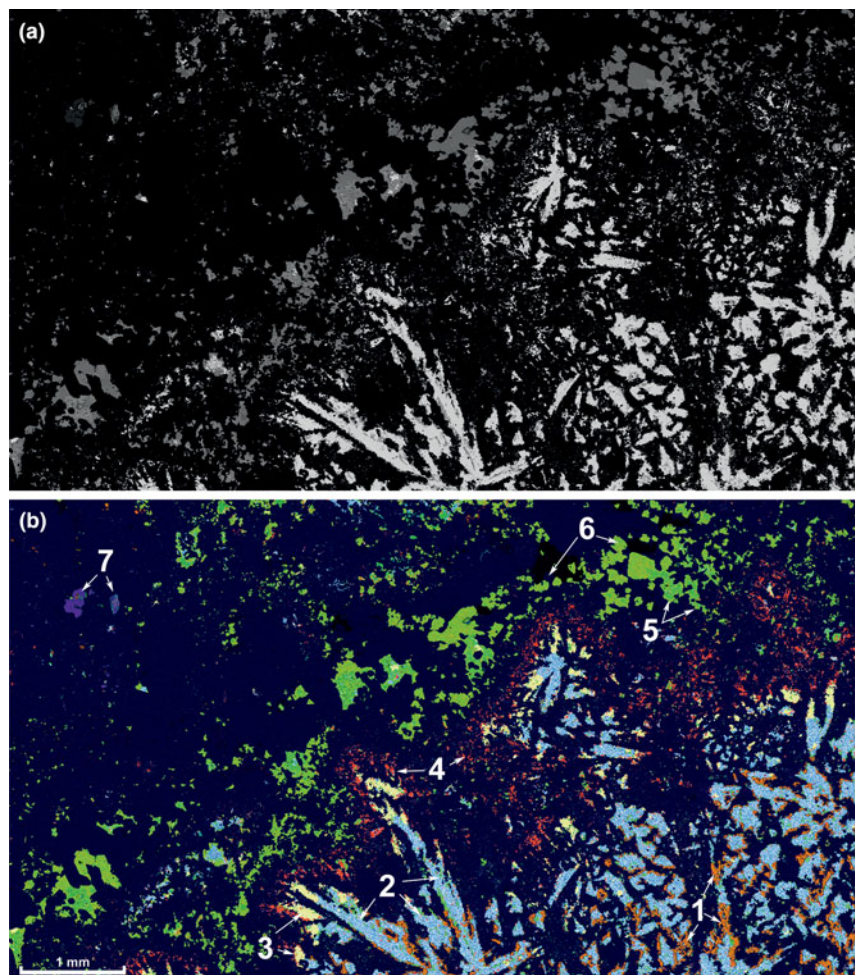


Fig. 4. SEM back-scattered electron image (a) and major minerals distribution map (b) of a banded Au-Te ore sample representing stages 2 and 3 of the mineral deposition cycle (Fig. 5). Minerals determined using EDS X-ray mapping. Sample db03-0044 (NHM catalogue number BM 2020,2), BAM zone. Legend for the mineral map (b): (1) Mn-bearing dolomite (orange); (2) tellurium (blue dots); (3) sylvanite (yellow); (4) kawazulite (red); (5) Te-Se bearing tennantite-tetrahedrite series (bright green); (6) tennantite-(Fe) (yellowish green); and (7) rutile + cassiterite in a quartz clast of the stage 1 (blue and reddish blue, respectively). Matrix (dark blue) – quartz.

Mineral	Alteration		Stages/Substages of ore deposition cycle				
	Argillisite / Acid-sulfate		1	2a	2b	3a	3b
Quartz							
Dickite	—						
Kaolinite	—						
Mn-Dolomite							
Pyrite		—					
Apatite-(F)	—						
Svanbergite-Woodhouseite Series	—	—					
Illite-Aluminoceladonite Series	—						
Rutile	—						
W-Sn-bearing rutile							
Anatase	—						
Zircon	—						
Sc-bearing Zircon							
Cassiterite							
W-Ga-V-Al-bearing Cassiterite							
Sheelite							
Svetlanaite (TL)							
Mohite							
Unnamed Cu ₂ Sn(Se,S) ₃							
Stannite							
Colusite							
Hemusite							
Kiddcreekite							
Mawsonite							
Chalcopyrite							
Tennantite-(Fe)							
Tennantite-Tetrahedrite Series							
Tetrahedrite Subgroup							
Goldfieldite Subgroup							
Unnamed PbCuSbSe ₃							
Altaite							
Claustalite							
Gold							
Sylvanite							
Cu-bearing Sylvanite							
Kostovite							
Hessite							
Stützite							
Rickardite							
Vulcanite							
Unnamed (Cu,Tl,Ag) sulfotelluride							
Unnamed Cu-Sn sulfotelluride							
Poubaite							
Tellurantimony							
Kawazulite							
Sb-bearing Kawazulite							
Unnamed (Sb,As) ₂ Te ₂ Se							
Tellurium							

Fig. 5. Formation stages and paragenetic sequence of minerals in Sn-bearing Au-Te bonanza ores.

in evaporation rates between H₂S, H₂Se and H₂Te from the boiling fluid.

Appearance, physical and optical properties

Svetlanaite forms tiny euhedral spindles (0.5–2 μm × 10–15 μm, possibly sections of thin plates) in quartz (Fig. 6) in close association with cassiterite, rutile, Se-mohite, Se-mawsonite, kiddcreekite, hemusite, native tellurium, kostovite and Se-bearing fahlores (Se-goldfieldite–Se(Bi)-tetrahedrite–Se-tennantite).

Svetlanaite is opaque with a metallic lustre. The mineral is brittle. The density calculated on the basis of the empirical formula is 6.08 g/cm³. In plane-polarised reflected light, svetlanaite is light grey in the natural assemblage of gangue and ore minerals,

pleochroic from white to cream and strongly anisotropic in shades of light blue, dark blue, khaki and orange–brown. It exhibits no internal reflections.

Reflectance measurements were made on synthetic SnSe in air relative to a WTiC standard using a J & M TIDAS diode array spectrometer attached to a Zeiss Axiotron microscope. The results in comparison with herzenbergite (SnS) are tabulated in (Table 1) and illustrated in Fig. 7.

Chemical composition

Chemical analyses were performed with an Oxford Instruments Aztec Energy Scanning Electron Microscope – Energy-Dispersive Spectroscopy (SEM-EDS) system with a X-Max80 SDD detector

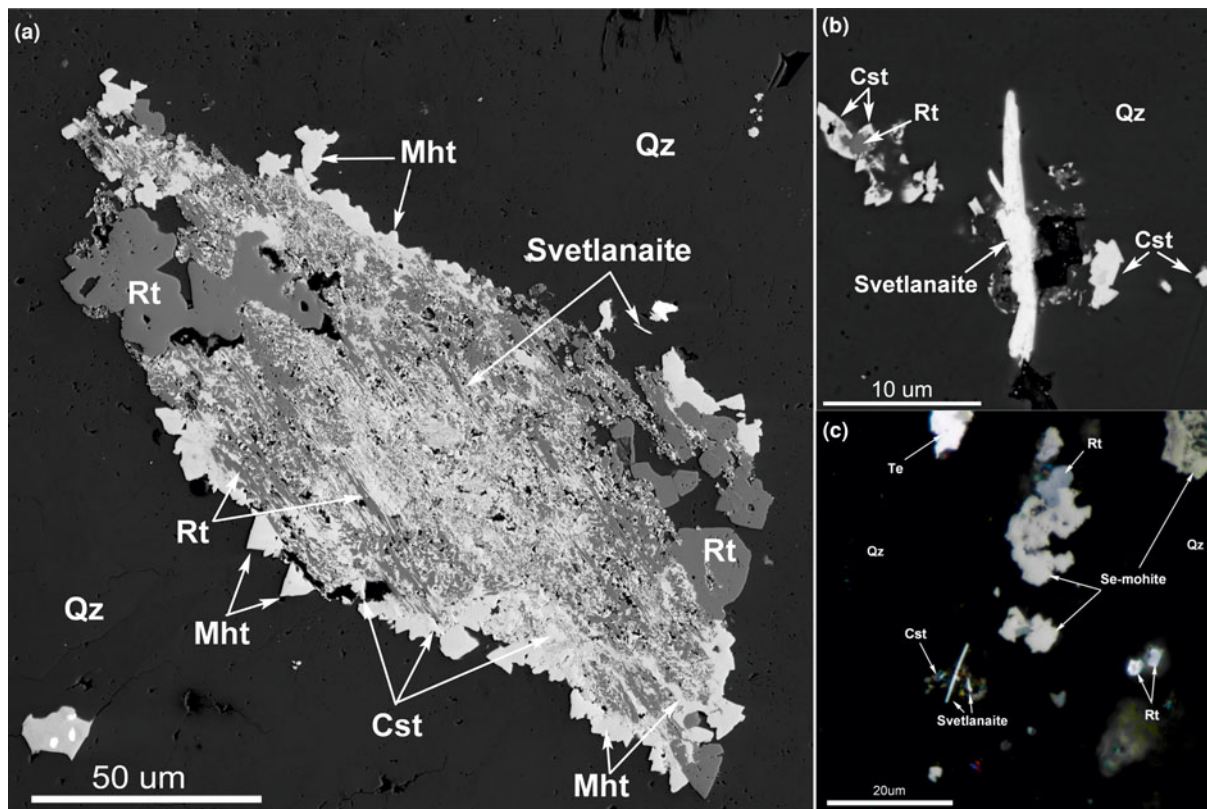


Fig. 6. (a) A complex intergrowth of rutile (Rt) and cassiterite (Cst) relics in an aggregate of mohoite (Mht) and svetlanaite (SnSe) in quartz (Qz). Back-scattered electron image, Sample 3. (b) Svetlanaite (SnSe) spindle crystal in quartz (black, Qz) with cassiterite (Cst). Back-scattered electron image, Sample 2. (c) Svetlanaite (SnSe) spindles in quartz with Se-bearing mohoite, rutile (Rt), cassiterite (Cst), and native tellurium (Te). Reflected light, Sample 1. Symbols according to Warr (2021).

Table 1. Reflectance data for synthetic analogue of svetlanaite, SnSe and comparison with herzenbergite (SnS).

λ (nm)	Synthetic SnSe		Herzenbergite (SnS)	
	R_1 (%)	R_2 (%)	R_1 (%)	R_2 (%)
400	52.0	53.5	45.9	52.9
420	51.4	54.2	45.6	53.6
440	51.0	54.9	45.2	53.8
460	50.9	56.0	44.6	53.15
470	50.9	56.5	44.2	52.6
480	50.9	57.0	44.0	52.2
500	50.9	57.3	43.7	51.25
520	50.7	57.2	43.65	50.6
540	50.3	56.8	43.2	49.9
546	50.2	56.7	43.0	49.6
560	50.0	56.3	42.3	48.8
580	49.6	55.6	41.4	47.6
589	49.5	55.3	41.05	47.1
600	49.3	55.0	40.7	46.6
620	49.1	54.3	40.3	45.75
640	48.8	53.7	40.0	45.0
650	48.7	53.4	40.0	44.7
660	48.6	53.1	39.9	44.25
680	48.3	52.6	39.55	43.7
700	48.1	52.2	39.3	43.1

Note: The values required by the Commission on Ore Mineralogy are given in bold.

and Inca Wave 500 wavelength-dispersive spectroscopy (WDS) system installed on a Tescan MIRA-3 SEM with a Shottky cathode located in the Tescan demo laboratory, Moscow, Russia. The

following conditions were applied for the data collection: acceleration voltage 10 kV; beam current 0.4 nA, beam diameter 0.1 μm ; wavelength dispersive spectrometer: acceleration voltage 10 kV; beam current 10 nA and beam diameter 1 μm . An accelerating voltage of 20 kV and 15 kV were also used to check for other possible elements present in the mineral. Qualitative WDS tests show that there are only three elements present – Sn, Se and S. There are no overlaps between X-ray lines of these elements and standard-based EDS was used for accurate quantitative analysis. A low beam current (0.4 nA) and low accelerating voltage (10 kV) were used in order to reduce electron beam interaction volume. The X-ray lines $\text{SnL}\alpha$, $\text{SeL}\alpha$ and $\text{SK}\alpha$ were used for quantification. The MAC (Micro-Analysis Consultants Ltd) set of pure elements (Sn, Se) and pure natural FeS_2 for S were used as standards. The 'XPP' exponential model of Pouchou and Pichoir (1991) was used for matrix correction.

Chemical analyses of the synthetic analogue were performed with a CAMECA SX-100 electron probe microanalyser (EPMA) in wavelength-dispersive mode using an electron beam focussed to 1–2 μm . Pure elements were used as standards. Concentrations were quantified on the $\text{SnL}\alpha$ and $\text{SeL}\alpha$ (with an overlap correction on $\text{SnL}\alpha_3$) lines with an accelerating voltage of 15 keV, and a beam current of 10 nA on the Faraday cup.

The results are given in Table 2. The empirical formulae of svetlanaite calculated on the basis of 2 atoms per formula unit is $\text{Sn}_{1.01}(\text{Se}_{0.92}\text{S}_{0.07})_{\Sigma 0.99}$ and $\text{Sn}_{1.00}\text{Se}_{1.00}$ for its synthetic analogue. The ideal formulae require Sn 60.05, Se 39.95, total 100 wt.%.

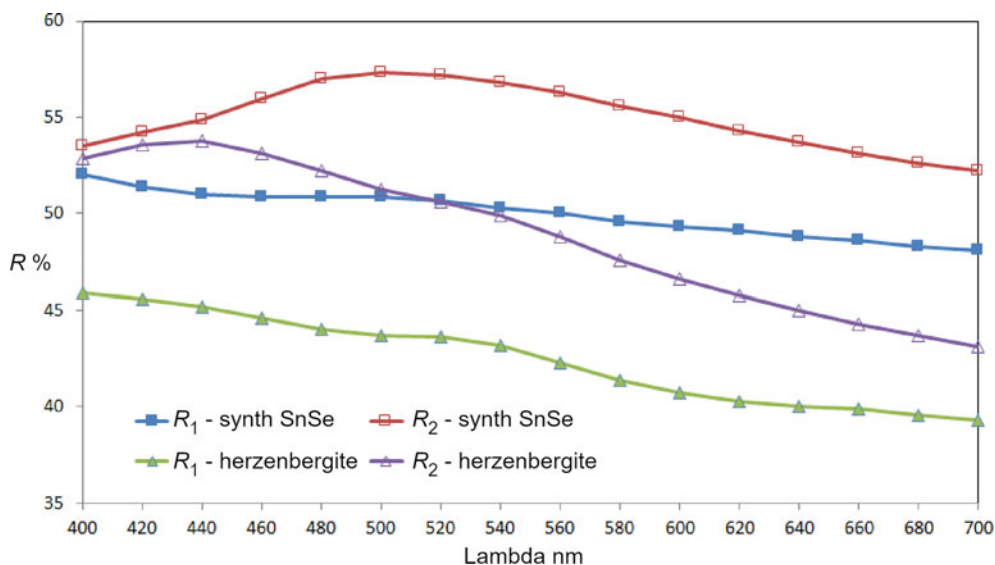


Fig. 7. Reflectance data for SnSe, the synthetic analogue of svetlanaite, in comparison with herzenbergite (SnS). The reflectance values ($R\%$) are plotted versus wavelength, λ , in nm.

Table 2. Electron-microprobe data from the grains of svetlanaite studied and its synthetic analogue.

Sample wt.%	Sn	Se	S	Total
Svetlanaite (n = 12)				
S20 133	61.70	35.99	1.58	99.27
S20 134	61.21	36.90	1.39	99.50
S20 135	60.50	37.28	0.71	98.48
s24 1	61.67	37.14	1.19	100.00
s24 2	63.16	33.66	3.19	100.01
s24 3	62.94	34.74	2.32	100.00
s27_1	60.60	38.36	1.04	100.00
s27_2	61.18	37.94	0.88	100.00
s27_3	60.85	38.53	0.62	100.00
s27_4	61.02	38.98	0.10	100.10
s27_12	59.29	40.71	0.10	100.10
s14_101	61.52	36.44	2.03	99.99
Average	61.30	37.22	1.26	99.79
Maximum	63.16	40.71	3.19	100.10
Minimum	59.29	33.66	0.10	98.48
Standard deviation	1.04	1.90	0.91	0.48
Synthetic SnSe (n = 7)				
Average	59.98	39.71		99.59
Maximum	60.31	39.86		
Minimum	59.64	39.65		
Standard deviation	0.20	0.07		
Ideal composition				
	60.05	39.95		100

Synthetic analogue

The size (0.5–2 $\mu\text{m} \times 10\text{--}15 \mu\text{m}$) of inclusions of svetlanaite, embedded in cassiterite or quartz, prevented its extraction and isolation in an amount required for relevant crystallographic and structural investigations. Therefore, these investigations were performed on the synthetic SnSe.

The synthetic phase SnSe was prepared in an evacuated and sealed silica-glass tube in a horizontal furnace in the Laboratory of Experimental Mineralogy of the Czech Geological Survey in Prague. To prevent loss of material to the vapour phase during the experiment, the free space in the tube was reduced by placing

Table 3. Powder X-ray diffraction data collection and Rietveld analysis for synthetic SnSe.

Data collection	
Radiation type, source	X-ray, CuK α
Generator settings	40 kV, 30 mA
Range in 2θ ($^\circ$)	10–110
Step size ($^\circ$)	0.01
Crystal data	
Space group	<i>Pnma</i> (62)
Unit-cell content	SnSe, $Z = 4$
Unit-cell parameters (Å)	$a = 11.500(2)$ $b = 4.154(2)$ $c = 4.445(2)$
Unit-cell volume (Å^3)	212.34(14)
Agreement factors (Rietveld refinement)	
R_{Bragg}	0.0517
R_p	0.1110
R_{wp}	0.1387
Weighting scheme	1/ y_0

a closely fitting silica glass rod against the charge. A charge of ~400 mg was carefully weighed out from the native elements. We used, as starting chemicals a tin ingot (99.9999% purity) and selenium pebbles (99.9999% purity). The evacuated tube with its charge was sealed and then annealed at 600°C for 1 week. After cooling by cold-water bath, the charge was ground into powder in acetone using an agate mortar, and thoroughly mixed to homogenise. The pulverised charge was sealed in an evacuated silica-glass tube again, and reheated at 200°C for 6 months. The experimental product was quenched rapidly in cold water.

X-ray crystallography

The powder X-ray diffraction pattern of synthetic SnSe, used for structure refinement, was collected in Bragg-Brentano geometry on a Bruker D8 Advance diffractometer, equipped with a LynxEye XE detector using CuK α radiation. Details of data collection and basic crystallographic data are in Table 3.

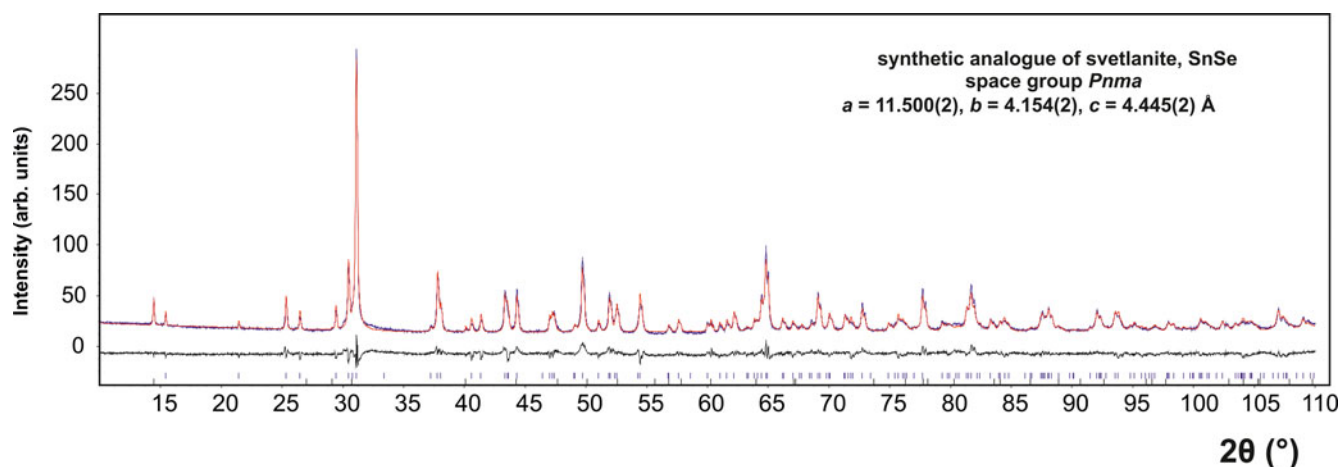


Fig. 8. The final Rietveld fit for SnSe, the synthetic analogue of svetlanite. In addition to SnSe, the sample contains 1.5 wt.% SnSe₂ as an impurity.

Table 4. Atomic positions (space group *Pnma*) and isotropic displacement parameters for the synthetic equivalent of svetlanite, SnSe. The isotropic displacement parameter (B_{iso}) was constrained to be equal for all atoms.

Atom	Wyckoff letter	x	y	z	B_{iso} [Å ²]
Sn	4c	0.11824(7)	¼	0.10078(4)	0.10(2)
Se	4c	0.85467(9)	¼	0.48780(6)	0.10(2)

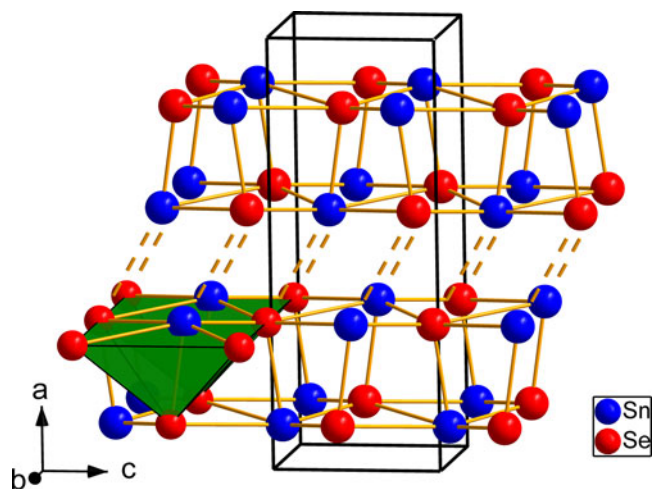


Fig. 9. Crystal structure of SnSe, the synthetic analogue of svetlanite showing the double-layers of Sn and Se atoms. The weak interactions between the double-layers are shown by dashed lines. The [SnSe₅] coordination pyramids (green) are shown in the left side of the figure.

The crystal structure of SnSe, the synthetic equivalent of svetlanite was refined using the Rietveld method by the *Topas 5* program (Bruker AXS, 2014). The crystal structure of SnSe by Sist *et al.* (2016) was used as an initial structure model in our Rietveld refinement (Fig. 8). The refined crystal coordinates did not deviate more than 0.005 from their initial values, and the structure model of Sist *et al.* (2016) was confirmed. The Rietveld refinement involved refinement of unit-cell parameters, crystal-structure coordinates, isotropic size and strain and isotropic displacement parameters. Correction for preferred orientation along [100] was applied (March–Dollas model). In total,

Table 5. Powder X-ray diffraction data of SnSe, the synthetic equivalent of svetlanite (CuK α radiation, Bruker D8 Advance, Bragg-Brentano geometry, fixed divergence slit). The powder pattern is affected by preferred orientation along [100].

$l_{\text{(obs)}}$	$l_{\text{(calc)}}$	$d_{\text{(obs)}}$	$d_{\text{(calc)}}$	h	k	l
5	4	5.750	5.750	2	0	0
1	1	4.144	4.145	1	0	1
4	4	3.516	3.516	2	0	1
1	1	3.367	3.367	2	1	0
1	2	3.034	3.035	0	1	1
14	14	2.934	2.934	1	1	1
100	100	2.874	2.875	4	0	0
14	10	2.378	2.379	3	1	1
2	2	2.221	2.222	0	0	2
1	1	2.182	2.181	1	0	2
10	8	2.086	2.087	4	1	1
8	6	2.042	2.042	5	0	1
1	1	1.931	1.931	1	1	2
1	1	1.920	1.922	3	0	2
19	16	1.833	1.833	5	1	1
1	1	1.788	1.788	2	2	1
4	4	1.759	1.758	4	0	2
2	1	1.741	1.740	6	1	0
2	3	1.683	1.683	4	2	0
1	1	1.598	1.598	5	0	2
1	1	1.504	1.504	1	2	2
1	1	1.491	1.491	5	1	2
1	1	1.455	1.456	5	2	1
2	2	1.444	1.444	7	1	1
18	22	1.437	1.437	8	0	0
4	4	1.358	1.358	8	1	0
1	1	1.342	1.342	4	2	2
1	1	1.321	1.321	7	0	2
1	2	1.299	1.299	8	1	1
5	5	1.228	1.228	9	0	1

The six strongest lines are given in bold.

13 parameters were refined. Background was determined by means of a Chebyshev polynomial of the 5th order. The final Rietveld plot is shown in Fig. 8. Table 4 shows atomic positions. Note we performed the refinement in the standard setting of the *Pnma* space group (No. 62). Contrary to that, Wiedemaier and Schnering (1978) carried out a refinement of synthetic SnSe in the space group setting *Pbnm*, as this setting was originally chosen by Zachariasen (1932) for this structure type. In order to make our results of refinement directly comparable with those of Sist *et al.*

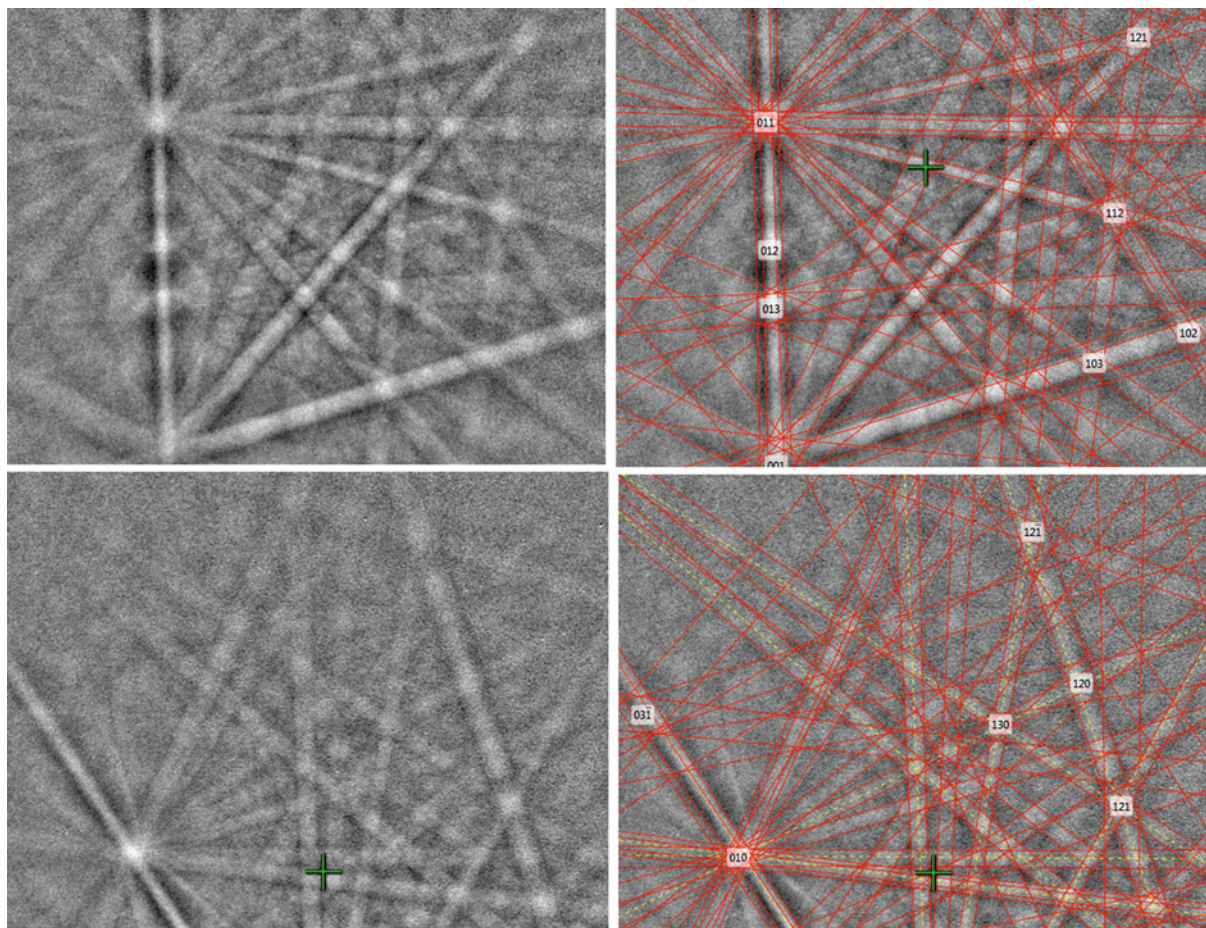


Fig. 10. Electron back-scattered diffraction patterns of natural SnSe; in the right pane the Kikuchi bands are solved (indexed).

(2016), we used the *Pnma* standard setting. The crystallographic information file has been deposited with the Principal Editor of *Mineralogical Magazine* and is available as Supplementary material.

Structure description

The synthetic analogue of svetlanaite, SnSe crystallises in the GeS-structure type. It is isostructural with the mineral herzenbergite (SnS). It crystallises in a layered structure with tightly bonded double layers running parallel to (100) which are separated by spaces accommodating the lone electron pair of Sn^{2+} atoms. Tin atoms show three short [2.748(1) Å and 2.7849(3) Å $\times 2$] and two longer [3.33548(3) Å $\times 2$] Se contacts forming [SnSe₅] coordination pyramids with a rectangular base (see Fig. 9). Whereas the double layer is held by a system of strong covalent bonds, the interaction between the double layers is considerably weaker [Sn–Se contacts at 3.485(1) Å] resulting in a perfect cleavage along the (100) plane. The Sn–Se bond distances in svetlanaite are slightly longer than the corresponding Sn–S distances observed in herzenbergite (three short 2.617–2.661 and two long 3.284 Å) by Chattopadhyay *et al.* (1986). This can be explained by the larger covalent radius of Se (1.20 Å) compared to S (1.05 Å). Note that the isostructural SnS is one of the archetypes used by Makovicky (1985) for the definition and description of families of sulfosalts. Its crystal structure can alternatively be viewed as a distortion derivative of PbS, however such

interpretation obscures the decisive role of stereochemically active lone electron pairs of Sn in this archetype (Makovicky, 2006).

Proof of identity of natural and synthetic svetlanaite

The structural identity of natural svetlanaite and its synthetic analogue was confirmed by electron back-scattering diffraction (EBSD) measurements on the natural sample and comparison of the structural model for SnSe from our Rietveld refinement and crystallographic data for synthetic SnSe available in the Inorganic Crystal Structure Database (FIZ, 2020).

A TESCAN LYRA3 FEG SEM combined with the EBSD system (Oxford Instruments AztecHKL with a NordlysNano EDSD detector) was used for the measurements. The sample surface was prepared for EBSD by polishing with colloidal silica followed by broad beam ion milling (Gatan PECS II argon ion beam system operated at 2 kV for 60 min). Acquisition conditions were: accelerating voltage 20 kV, beam current 0.4 nA and no binning (full EBSD resolution is 1344 \times 1024). Indexing conditions were: refined accuracy mode, 12 bands and 60 reflectors. A search of the Inorganic Crystal Structure Database (FIZ, 2020) found three crystal modifications existing for synthetic SnSe: (1) SnSe (*Pnma*) GeS-structure type, card no. 244268; (2) SnSe (*Cmcm*) TII-structure type, card no. 52423; and (3) SnSe (*Fm $\bar{3}m$*) NaCl-structure type, card no. 76032.

The best fit (with mean angle deviation (MAD) from 0.29 to 0.46° and five determinations) was obtained for the *Pnma* structure with crystallographic data from our refinement of synthetic SnSe (see Table 5), and is shown in Fig. 10. The fit for the *Cmcm* structure (Chattopadhyay et al., 1986) resulted in a significantly much poorer fit (MAD 0.83–0.87°) and the *Fm $\bar{3}$ m* structure (Palatnik and Levitin, 1954) did not fit at all. This is in accordance with the assumed temperature of formation of svetlanaite at ~200–300°C, as the *Cmcm* structure represents high-temperature modifications (above 533°C) of SnSe (Wiedemeier and Csillag, 1979). The cubic structure of synthetic SnSe reported by Palatnik and Levitin (1954) is questionable, as synthetic SnSe melts before its possible transformation to the NaCl-structure type (Wiedemeier and Schnering, 1978).

Summary and concluding remarks

Svetlanaite is a new mineral found in quartz veins of the high-sulfidation epithermal Au deposit at Ozernovskoe, Kamchatka, Russia. It occurs in an association with a wide range of Sn-, W- and Mo- bearing sulfides and sulfoselenides, tellurides and selenotellurides. Svetlanaite was most likely formed at ~200–300°C, under conditions of increasing pH and low fugacity f_{S_2} . Svetlanaite has the GeS-type structure and is isostructural with herzenbergite (SnS).

Acknowledgements. The authors acknowledge Ritsuro Miyawaki, Chairman of the CNMNC and its members for helpful comments on the submitted data. The comments made by Ernst M. Spiridonov, an anonymous reviewer, Structures editor Peter Leverett, Associate Editor Elena Zhitova and the Principal Editor Stuart Mills are greatly appreciated. This work was supported by the Czech Geological Survey (DKRVO/ČGS 2018–2022) and by the Grant Agency of the Czech Republic (project No. 22-26485S to A.V.). CJS acknowledges Natural Environment Research Council grant NE/M010848/1 Tellurium and Selenium Cycling and Supply. VK acknowledges Tescan Ltd. for opportunity to use Tescan SEMs and Oxford Instruments analytical equipment in their demo laboratory in Moscow.

Supplementary material. To view supplementary material for this article, please visit <https://doi.org/10.1180/mgm.2021.80>

References

- Bruker AXS (2014) *Topas 5, Computing Program*. Bruker AXS GmbH, Karlsruhe, Germany.
- Chattopadhyay T., Pannetier J. and von Schnering H.G. (1986) Neutron diffraction study of the structural phase transition in SnS and SnSe. *Journal of Physics and Chemistry of Solids*, **47**, 879–885.
- Demin A.G. (2015) Ozernovskoye field as a new promising ore object of Central Kamchatka with complex ores for gold, tungsten, silver and copper. *Zoloto i tekhnologii*, **1**, 12 [in Russian].

- FIZ Karlsruhe (2020) *Inorganic Crystal Structure Database (ICSD)*. FIZ Karlsruhe, Eggenstein-Leopoldshafen, Germany [<https://icsd.products.fiz-karlsruhe.de/>].
- Kovalenker V.A. and Plotinskaya O.Y. (2005) Te and Se mineralogy of Ozernovskoe and Prasolovskoe epithermal gold deposits, Kuril–Kamchatka volcanic belt. *Geochemistry, Mineralogy and Petrology (Sofia)*, **43**, 118–124.
- Litvinov A.F., Patoka M.G. and Markovsky B.A. (editors) (1999) *Map of Mineral Resources of Kamchatka Region, Explanatory Memorandum and Legend*. St. Petersburg, Ministry of Natural Resources of the Russian Federation, Natural Resources Committee of Kamchatka Region and Koryak Autonomous Area, VSEGEI, 1 map on 18 sheets, scale 1:500,000, 563 pp. [in Russian and English].
- Makovicky E. (1985) The building principles and classification of sulphosalts based on the SnS archetype. *Fortschritte der Mineralogie*, **63**, 45–89.
- Makovicky E. (2006) Crystal structures of sulfides and other chalcogenides. Pp. 7–125 in: *Sulfide Mineralogy and Geochemistry* (Vaughan, D.J., editor). Reviews in Mineralogy and Geochemistry, 61. Mineralogical Society of America and the Geochemical Society, Chantilly, Virginia, USA.
- Naumova O.A. (1995) *Hydrothermally Altered Rocks of Gold-Silver Deposits of Central and Southern Kamchatka*. *Canad. Sci. (Geol.-Mineral.) Dissertation*, TsNIGRI [Central Research Institute of geological prospecting for base and precious metals], Moscow.
- Okrugin V.M., Vymazalová A., Kozlov V.V., Laufek F., Stanley C.J. and Shkilsky I. (2020) Svetlanaite, IMA 2020-013. CNMNC Newsletter No. 56. *Mineralogical Magazine*, **84**, 623–627.
- Palatnik L.S. and Levitin V.V. (1954) X-ray investigation of alloys Sn–Se, Zn–Se, Cd–Se and Ag–Se. *Doklady Akademii Nauk SSSR*, **96**, 975–978.
- Petrenko I.D. (1999) *Gold-silver Formation of Kamchatka*. VSEGEI (Geological Research Institute), St. Petersburg, 115 pp. [in Russian].
- Pouchou J.L. and Pichoir F. (1991) Quantitative analysis of homogeneous or stratified microvolumes applying the model “PAP”. Pp. 31–75 in: *Electron Probe Quantification* (Heinrich, K.F.J. and Newbury, D.E., editors). Plenum Press, New York.
- Sist M., Zhang J. and Brummerstedt Iversen B. (2016) Crystal structure and phase transition of thermoelectric SnSe. *Acta Crystallographica*, **B72**, 310–6.
- Spiridonov E.M., Ignatov A.I. and Shubina E.V. (1990) The evolution of fahlores from the Ozernovskoe volcanogenic deposit (Kamchatka). *Izvestia Academy of Sciences USSR, Geology series*, **9**, 82–94 [in Russian].
- Strunz H. and Nickel E.H. (2001) Class 2. SULFIDES and SULFOSALTS. Pp. 56–147 in: *Strunz Mineralogical Tables 9th Edition*. E. Schweizerbart'sche Verlagsbuchhandlung (Nägele u. Obermiller), Stuttgart, Germany.
- Vakin M.E. and Naumova O.A. (1994) Geological structural position and frameworks of localization of bonanza ores at the Ozernovskoe gold-silver deposit (Kamchatka). *Rudy i Metally*, **2**, 97–104 [in Russian].
- Warr L.N. (2021) IMA–CNMNC approved mineral symbols. *Mineralogical Magazine*, **85**, 291–320.
- Wiedemeier H. and Csillag H.J. (1979) The thermal expansion and high temperature transformation of SnS and SnSe. *Zeitschrift für Kristallographie*, **148**, 17–29.
- Wiedemeier H. and von Schnering H.G. (1978) Refinement of the structures of GeS, GeSe, SnS and SnSe. *Zeitschrift für Kristallographie*, **148**, 295–303.
- Zachariasen W.H. (1932) The crystal lattice of germano sulphide, GeS. *Physical Reviews*, **40**, 917–922.